The dynamics of wettability driven droplets in smooth and corrugated microchannels

J. Stat. Mech. (2012) P10005

(http://iopscience.iop.org/1742-5468/2012/10/P10005)

Journal of Statistical Mechanics: Theory and Experiment
An IOP and SISSA journal

The dynamics of wettability driven droplets in smooth and corrugated microchannels

E Esmaili, A Moosavi[1] and A Mazloomi

Department of Mechanical Engineering, Sharif University of Technology, Azadi Avenue, PO Box 11365-9567 Tehran, Iran
E-mail: esmaili@mech.sharif.edu, moosavi@sharif.edu and Ali_Mazloomi@mech.sharif.edu

Received 12 June 2012
Accepted 12 September 2012
Published 4 October 2012

Online at stacks.iop.org/JSTAT/2012/P10005
doi:10.1088/1742-5468/2012/10/P10005

Abstract. A multi-component lattice Boltzmann scheme is used to investigate the dynamics of a wettability driven droplet within a microchannel. The driving force for the motion is created by a stepwise change in the wettability of the channel walls. Moreover, an analytical solution is developed for evaluation of the dynamics of the droplet inside the channel. The effects of various parameters such as the height of the channel, the wetting pattern of the channel walls, the viscosity and the density ratio on the dynamics are studied. Also, the effect of grooves of different sizes on the channel surfaces on the dynamics of the droplet is investigated for both hydrophilic and hydrophobic surfaces. Finally, the effect of an obstacle in the channel on the motion of the droplet is studied. The numerical results are compared with the analytical solutions and close agreement between the results is found.

Keywords: microfluidics and nanofluidics (theory), fluids in confined geometries, interfacial phenomena and wetting, lattice Boltzmann methods

---

[1] Author to whom any correspondence should be addressed.

1742-5468/12/P10005+21$33.00

Contents

1. Introduction 2

2. The numerical method 4

3. The analytical solution 5

4. Results and discussion 7
   - 4.1. The chemical step case with $\theta_1 = \theta_4$ and $\theta_2 = \theta_3$ . . . 9
     - 4.1.1. The effect of channel height. . . . 9
     - 4.1.2. The effect of surface wettability and the contact angle. . . . 11
     - 4.1.3. The effect of viscosity. . . . 11
   - 4.2. The chemical step case with $\theta_2 \neq \theta_3 \neq \theta_4$ and $\theta_1 = \theta_4$ . . . 12
   - 4.3. The effect of grooves . . . 14
     - 4.3.1. The chemical step on both the channel walls ($\theta_1 = \theta_4$ and $\theta_2 = \theta_3$). . . 14
     - 4.3.2. The chemical step on the top wall ($\theta_1 = \theta_2$). . . . 17
   - 4.4. The effect of obstacles on the dynamics ($\theta_1 = \theta_4, \theta_2 = \theta_3$) . . . 17

5. Conclusion 18

References 20

1. Introduction

Research concerning the transport of droplets inside microchannels is relevant for various applications. For example, droplets can be used for feeding micromotors, in lab-on-a-chip instruments and for sampling the materials in biological applications [1, 2]. Advances in micromanufacturing and nanomanufacturing have created the possibility of using more efficient methods to transport droplets.

In conventional methods such as applying a pressure gradient, the force required to transport the droplets substantially increases at small scales, as in these systems the surface to volume ratio is very large and the Reynolds and capillary numbers are small [3]. However, a change in the wettability of the channel walls can be used to drive droplets inside the channels [3, 4]. It is well known that if a droplet is positioned on the boundary of two parts of a chemical step, since the equilibrium contact angle of the droplet on the parts is not equal, a net surface force is created that is able to drive the droplet [5]–[8]. In this manner it is possible to produce a continuous motion inside the channel by providing a chemical gradient [5, 6, 8, 9]. There are various experimental techniques for providing a wettability change on a surface. These methods include surface coating [10], irradiation [11], electrochemical operations [12] and applying surfactants [13]. A chemical step is a pattern that because of its simplicity of production and its application in various systems has been given attention [14]. A chemical step can easily be produced by covering a part of a wettable surface with a non-wettable material [14].

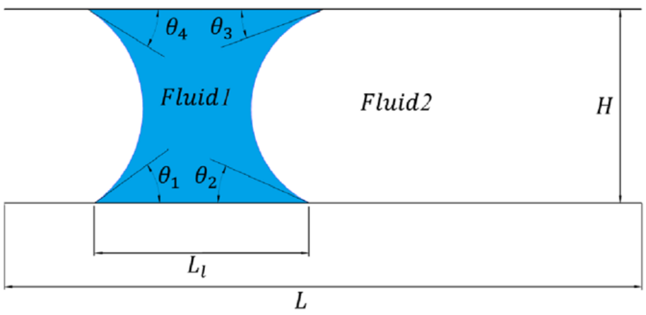

Figure 1. A schematic representation of the problem. A 2D droplet (fluid 1) with length L_1 under chemical steps on the top and bottom walls is moving within a channel with length L. The contact angle of the droplet is equal to θ_1 (bottom left), θ_2 (bottom right), θ_3 (top right) and θ_4 (top left).

The dynamics of droplets on chemically or topographically structured substrates has been investigated via various numerical techniques [3, 9]. The lattice Boltzmann method (LBM) has also been used to study droplets on the structured substrates [14, 16, 17, 34]. The motivation for applying LBM for such problems stems from the fact that the LBM because of its inherent kinetic nature can efficiently handle complex interfaces and geometries. Moreover, there is no need to consider any assumption for the relation between the contact angle and the contact line velocity because coalescence of the contact line is naturally treated by this method. The dynamics of droplets on chemical surfaces with different forms of wettability patterns has been studied via the lattice Boltzmann method in [18]. In the study the effect of frequency of wettability changes, and positions and conditions of the droplets have been determined and discussed [18]. Droplet coalescence driven by wettability gradients is also investigated in [19] and the velocity field and mechanism of the droplet motion are illustrated. Studying the effect of a constant volumetric force on a droplet situated in a channel with a chemical surface has been an effort in this direction. In addition, the effects of the wettability gradient and roughness gradient have been investigated numerically via the lattice Boltzmann method and experimentally [34].

As already stated, wetting on the surfaces can have substantial effects on the dynamics of the droplets at the microscale and nanoscale. In addition, topographic heterogeneities on the surfaces can considerably affect the dynamics. For single-phase systems it is shown that the flow rate is influenced considerably by the number, size, and shape of the grooves [20]. Also the presence of grooves can appreciably improve mixing in microdevices [21]. For two-phase systems there are various numerical researches via LBM that consider the effect of topographical patterns on the droplet spreading [16, 17, 22]. The motion of the contact line on topographic substrates is investigated in [23]. The results indicate that the dynamic contact angles change periodically between two maximum and minimum values and the velocity is a function of the surface topology. The behavior and dynamics of droplets under a volumetric force on different heterogeneous surfaces have been investigated in [24, 25].

In the present study we use the lattice Boltzmann method and thoroughly study the dynamics of 2D droplets inside microchannels. The droplets are driven by an abrupt wettability change (a chemical step) on the surfaces of the channels. As depicted in figure 1 we consider the cases in which the top and bottom walls have different contact angles. We also present an analytical solution for the problem. The effect of the viscosity ratio on the dynamics, the acceleration process and its dependence on the density ratio of the fluids, and the estimation of the travel time of the droplets will be investigated. Also in the present study the effect of topographic heterogeneities in the form of grooves on the velocity and the drag force exerted on the droplets will be inspected for both the hydrophilic and hydrophobic surfaces. In addition, the dynamics of droplets in the presence of an obstacle will be studied.

2. The numerical method

In this section the Shan–Chen multi-component lattice Boltzmann method is introduced briefly [26, 27]. For any component k the lattice Boltzmann equation, which contains two steps of collision and streaming, is given as

$$f_a^k(x+e_a\Delta t, t+\Delta t) = f_a^k(x,t) - \frac{\Delta t}{\tau_k}[f_a^k(x,t) - f_a^{k(\mathrm{eq})}(x,t)], \tag{1}$$

where the distribution function $f_a^k(x,t)$ is a scalar quantity which describes the probability of finding a fluid particle at location x in the direction a and at the time t for the kth component. Therefore it has a real and non-negative value. Δt represents the time increment. In the right-hand side of the equation, τ_k is the relaxation time of the kth component in lattice units which is related to the kinematic viscosity as follows:

$$\nu_k = c_s^2(\tau - 0.5) \tag{2}$$

where $c_s^2 = 1/3$. In addition, $f_a^{k(\mathrm{eq})}(x,t)$ in the right-hand side is the equilibrium distribution function and is obtained from the following relation:

$$f_a^{k(\mathrm{eq})} = w_a\rho_a\left[1 + \frac{\mathbf{e}_a\cdot\mathbf{u}_k^{\mathrm{eq}}}{c_s^2} + \frac{(\mathbf{e}_a\cdot\mathbf{u}_k^{\mathrm{eq}})^2}{2c_s^4} - \frac{u_k^{eq^2}}{2c_s^2}\right] \tag{3}$$

where $\rho_k = \sum_a f_a^k$ is the macroscopic density for the kth component, and the $\mathbf{e}_a$ represent the discrete velocities and for a D_2Q_9 lattice are given by

$$\mathbf{e}_a = \begin{cases} (0,0) & a=0 \\ \left(\cos\dfrac{(a-1)\pi}{2}, \sin\dfrac{(a-1)\pi}{2}\right) & a=1-4 \\ \sqrt{2}\left(\cos\left[\dfrac{(a-5)\pi}{2}+\dfrac{\pi}{4}\right], \sin\left[\dfrac{(a-5)\pi}{2}+\dfrac{\pi}{4}\right]\right) & a=5-8. \end{cases} \tag{4}$$

In equation (3) the w_a are the weight coefficients associated with the lattice and for a D_2Q_9 lattice have the following values:

$$w_a = \begin{cases} 4/9 & a=0 \\ 1/9 & a=1,2,3,4 \\ 1/36 & a=5,6,7,8. \end{cases} \tag{5}$$

Also in equation (3) the equilibrium velocity of the kth component $\mathbf{u}_k^{\mathrm{eq}}$ can be calculated from

$$\mathbf{u}_k^{\mathrm{eq}} = \mathbf{u}' + \frac{\tau_k \mathbf{F}_k}{\rho_k}, \tag{6}$$

where u' is a common velocity that is added to the equilibrium velocity of each part and is given by

$$u' = \left(\sum_k \frac{\rho_k \mathbf{u}_k}{\tau_k}\right) \Big/ \left(\sum_k \frac{\rho_k}{\tau_k}\right), \tag{7}$$

with $\mathbf{u}_k$ the macroscopic velocity ($\rho_k \mathbf{u}_k = \sum_a \mathbf{e}_a f_a^k$). In equation (6) $\mathbf{F}_k$ is the total force exerted on the kth component which includes both the fluid–fluid cohesion (F_k^{c}) and the fluid–solid adhesion F_k^{ads}, i.e.,

$$F_k = F_k^{\mathrm{c}} + F_k^{\mathrm{ads}}. \tag{8}$$

The total fluid–fluid interaction force at any position $\mathbf{x}$ is given by [28]

$$F_k^{\mathrm{c}}(x) = -G_{\mathrm{c}} \rho_k(x,t) \sum_a w_a \rho_{\bar{k}}(\mathbf{x} + \mathbf{e}_a \Delta t, t)\mathbf{e}_a, \tag{9}$$

where G_{c} is a parameter that controls the adhesion force and $\bar{k}$ is the other component. The force exerted by the wall surface is given by [28]

$$F_k^{\mathrm{ads}}(x,t) = -G_{\mathrm{ads},k} \rho_k(x,t) \sum_a w_a s(\mathbf{x} + \mathbf{e}_a \Delta t)\mathbf{e}_a, \tag{10}$$

where $G_{\mathrm{ads},k}$ represents the strength of interaction between the fluid and the solid and s is an indicator function which is equal to 1 and 0 for solids and fluids, respectively. On this basis, by adjusting the parameters it is possible to model different contact angles (see [29]). The pressure of the total fluid is equal to $p = (\rho_1 + \rho_2)/3 + G_{\mathrm{c}} \rho_1 \rho_2 / 3$ [29, 31]. Using Chapman–Enskog expansion [32] the following continuity and momentum equations can be obtained for the fluid mixture as a single fluid [33]:

$$\frac{\partial \rho}{\partial t} + \nabla \cdot (\rho \mathbf{u}) = 0, \tag{11}$$

$$\rho \left[\frac{\partial \rho}{\partial t} + (\mathbf{u} \cdot \nabla)\mathbf{u}\right] = -\nabla p + \nabla \left[\mu(\nabla \cdot \mathbf{u} + \mathbf{u} \cdot \nabla)\right] + \rho \mathbf{g}, \tag{12}$$

where $\rho = \sum_k \rho_k$ is the density of the fluid mixture and the velocity of the fluid mixture is given by $\rho \mathbf{u} = \sum_k \rho_k \mathbf{u}_k + \frac{1}{2} \sum_k \mathbf{F}_k$. The dynamic viscosity is given by $\mu = \sum_k \mu_k$.

3. The analytical solution

Considering the importance of the investigations on wettability driven droplets in microchannels, finding an analytical solution would be very helpful. Also given the limitations of the original Shan–Chen multi-component model, which is not able to simulate two fluids with high density and viscosity ratio, it is necessary to determine the density and viscous effects of the gas phase on the dynamics [33]. In figure 1 the overall schematic representation of the problem is shown. A channel with height H and

J. Stat. Mech. (2012) P10005

length L is considered. The fluid 1 with length L_1 is placed at the start of the channel. A bounce-back boundary condition is applied to the top and bottom walls. A periodic boundary condition is also applied to the left and right sides of the channel. In order to consider the effects of both fluids the momentum equation for both fluids will be given as [33]

$$\frac{\mathrm{d}(m_{\mathrm{g}}u_{\mathrm{g}}+m_{\mathrm{l}}u_{\mathrm{l}})}{\mathrm{d}t}=F_{\mathrm{driv}}+F_{\mathrm{visc}}. \tag{13}$$

Due to the periodicity of the boundaries on the sides of the channel the total mass of the system is conserved. Also with the incompressibility assumption the right side of equation (13) will be simplified as follows:

$$\begin{aligned}F_{\mathrm{driv}}+F_{\mathrm{visc}}&=\gamma(\cos\theta_2-\cos\theta_1)+\gamma(\cos\theta_3-\cos\theta_4)\\&\quad-2\left(\mu_{\mathrm{l}}L_{\mathrm{l}}\frac{\partial u}{\partial y}\bigg|_{y=0}-\mu_{\mathrm{g}}(L-L_{\mathrm{l}})\frac{\partial u}{\partial y}\bigg|_{y=0}\right),\end{aligned} \tag{14}$$

where γ represents the surface tension. Assuming Poiseuille flow, namely, $u(y)=6\bar{u}y(H-y)/H^2$ for both fluids, where $\bar{u}$ is the average velocity, equation (13) is reduced to the following differential equation:

$$[\rho_{\mathrm{l}}L_{\mathrm{l}}+\rho_{\mathrm{g}}(L-L_{\mathrm{l}})]\dot{u}+\frac{12}{H^2}\left[\rho_{\mathrm{l}}\nu_{\mathrm{l}}L_{\mathrm{l}}+\rho_{\mathrm{g}}\nu_{\mathrm{g}}(L-L_{\mathrm{l}})\right]u=\frac{\gamma(\Delta\cos\theta_{21}-\Delta\cos\theta_{34})}{H}, \tag{15}$$

where ν_{l} and ν_{g} are kinematic viscosities of the liquid (fluid 1) and the gas (fluid 2). L_{l} stands for the droplet length. By solving the differential equation (15), the velocities and positions of the droplet during the motion can be obtained. We will examine the validity of the parabolic profile assumption in the subsequent sections. To solve this equation two initial conditions are required. We assume that

$$x(0)=0 \qquad \text{and} \qquad u(0)=0. \tag{16}$$

It can be shown that the solution of the equation (15) can be given by the following expressions:

$$x_{\mathrm{l}}(t)=\frac{\gamma H(\Delta\cos\theta_{21}+\Delta\cos\theta_{34})}{12[\rho_{\mathrm{l}}\nu_{\mathrm{l}}L_{\mathrm{l}}+\rho_{\mathrm{g}}\nu_{\mathrm{g}}(L-L_{\mathrm{l}})]}t_s(\mathrm{e}^{-t/t_s}+t/t_s-1), \tag{17}$$

$$u(t)=\frac{\gamma H(\Delta\cos\theta_{21}+\Delta\cos\theta_{34})}{12[\rho_{\mathrm{l}}\nu_{\mathrm{l}}L_{\mathrm{l}}+\rho_{\mathrm{g}}\nu_{\mathrm{g}}(L-L_{\mathrm{l}})]}(-\mathrm{e}^{-t/t_s}+1), \tag{18}$$

where $t_s=H^2a/(12b)$ with a and b given by

$$a=\rho_{\mathrm{l}}L_{\mathrm{l}}+\rho_{\mathrm{g}}(L-L_{\mathrm{l}}) \tag{19}$$

$$b=\rho_{\mathrm{l}}\nu_{\mathrm{l}}L_{\mathrm{l}}+\rho_{\mathrm{g}}\nu_{\mathrm{g}}(L-L_{\mathrm{l}}) \tag{20}$$

$$\Delta\cos\theta_{21}=\cos\theta_2-\cos\theta_1 \tag{21}$$

$$\Delta\cos\theta_{34}=\cos\theta_3-\cos\theta_4. \tag{22}$$

Equations (17) and (18) suggest that the dynamics of the droplet depends more on the viscosities than on the densities (the densities appear in the exponential term). As can be seen, the density ratio of the fluids only appears in a part related to the acceleration of the droplet (exponential terms in equations (17) and (18)). Such a behavior can also be

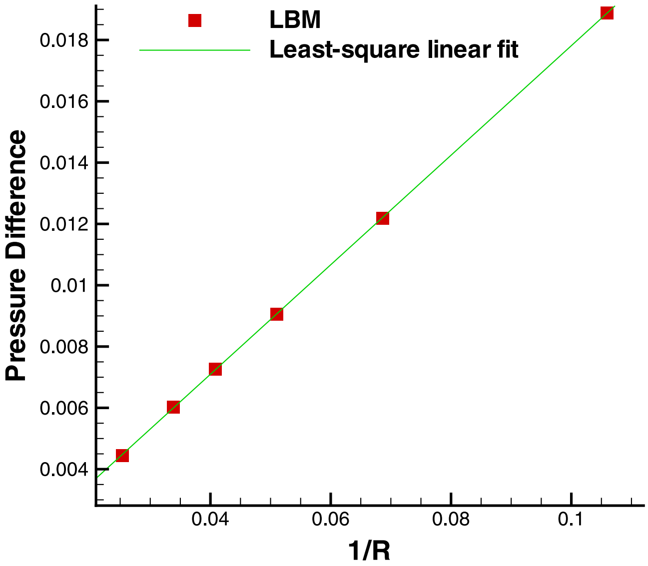

Figure 2. Pressure difference between inside and outside the droplet versus the inverse of the droplet radius, used to calculate the surface tension and for checking the Laplace equation ($\Delta p = \gamma/R$). $\rho_{\mathrm{l}} = \rho_{\mathrm{g}} = 2$ and $\mu_{\mathrm{l}} = \mu_{\mathrm{g}} = 1/6$ and $G_{\mathrm{c}} = 0.9$.

observed in capillary rising phenomena [33]. Considering equation (17) equal to $L_{\mathrm{l}}/2$, the total time of the droplet motion from the step can be calculated.

4. Results and discussion

Before considering different cases for the investigation it would be helpful to check the accuracy and reliability of the method. Calculation of the surface tension and the contact angle is very important in studying and analyzing droplets in different flows. In order to calculate the surface tension and verify the Laplace equation ($\Delta p = \gamma/R$), in our simulations a droplet in a 100×100 domain is considered. A periodic boundary condition is applied to all the boundaries [26, 28]. The simulations were carried out for different radii of the droplet. The results of the simulations for the droplet with $\rho_{\mathrm{l}} = \rho_{\mathrm{g}} = 2$ and $\mu_{\mathrm{l}} = \mu_{\mathrm{g}} = 1/6$ and $G_{\mathrm{c}} = 0.9$ are depicted in figure 2. The slope calculated from the diagram of figure 2 is equal to 0.1786 which is in complete agreement with the results reported in [29]. We also calculated the surface tension via a different method. For a plane interface it is shown that the surface tension can be given by [30]

$$\gamma = \int p_{yy} - p_{xx}\,\mathrm{d}y \tag{23}$$

where the subscripts x and y refer to the transversal and the normal to the interface and the pressure tensor is given by

$$\begin{aligned} p_{ij} = c_s^2 \left[\rho_1 + \rho_2 + G_{\mathrm{c}}\rho_1\rho_2 + c_s^2 \frac{G_{\mathrm{c}}}{2}\rho_1\Delta\rho_2 + c_s^2 \frac{G_{\mathrm{c}}}{2}\rho_2\Delta\rho_1 + c_s^2 \frac{G_{\mathrm{c}}}{2}(\nabla\rho_1 \cdot \nabla\rho_2) \right] \delta_{ij} \\ - c_s^4 G_{\mathrm{c}} \nabla\rho_1 \nabla\rho_2 + K_{ij}^{\tau} \end{aligned} \tag{24}$$

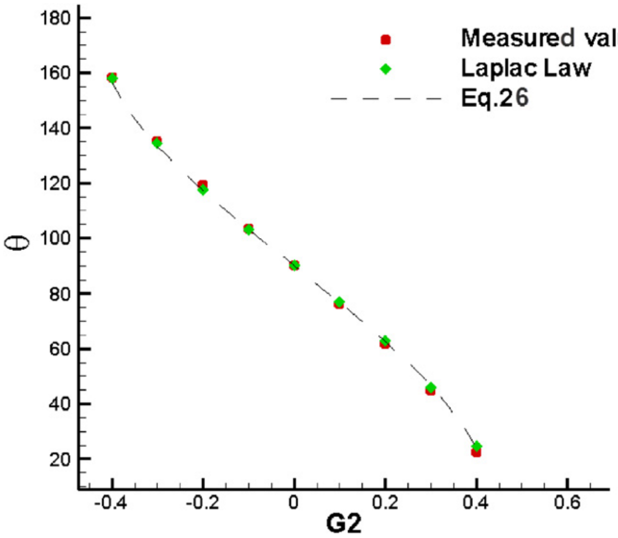

Figure 3. A comparison between the contact angles derived from equation (23), the Laplace equation ($\Delta p = (2\gamma\cos\theta)/H$) and the density contours. The channel dimension is equal to 400 × 60. $\rho_{\mathrm{l}} = \rho_{\mathrm{g}} = 2$ and $\mu_{\mathrm{l}} = \mu_{\mathrm{g}} = 1/6$ and $G_{\mathrm{c}} = 0.9$.

with K^{τ}_{ij} given as

$$K^{\tau}_{ij} = c_s^4 \frac{\rho_1\rho_2}{\rho}(\tau - 0.5)^2 \left(\frac{\partial_i\rho_1}{\rho_1} - \frac{\partial_i\rho_2}{\rho_2}\right)\left(\frac{\partial_j\rho_1}{\rho_1} - \frac{\partial_j\rho_2}{\rho_2}\right). \tag{25}$$

The value calculated for the surface tension from this method is equal to 0.1757 which is very close to that derived from the above derived value.

Calculation of the equilibrium contact angle of the droplets in the Shan–Chen model is another way of checking the accuracy of the simulation results. The geometry consists of a 400 × 60 domain as depicted in figure 1. A droplet with an initial configuration in the form of a rectangle is considered inside the channel. The fluid properties such as the density and viscosity are the same as for the previous case (calculating the surface tension). Recently a relation for evaluating the contact angle in the Shan–Chen model was proposed which can yield acceptable results [29]. This relation is suggested for the cases where the viscosities of the fluids are equal. However, this relation can still predict the contact angle for the cases with a change in the viscosity reasonably well [35]. This relation is given as [29]

$$\cos\theta_1 = \frac{G_{\mathrm{ads},2} - G_{\mathrm{ads},1}}{G_{\mathrm{c}}((\rho_{1,m} - \rho_{2,d})/2)}, \tag{26}$$

where the subscripts m and d stand for the main and dissolved densities, respectively. It should be noted that in all the simulations the coefficient of interaction of each component with the walls (both the top and bottom walls) is selected as $G_2 = -G_1$ because in this case the results of the simulation are more consistent with equation (26) [29]. In figure 3 the calculated contact angles for the droplet inside the channel from the density contour, the Laplace equation and equation (26) are compared. It is evident from the figure that the results obtained from the density contour and the Laplace equation are in excellent agreement. Also for the case studied the results show a very close compliance with equation (26). In [29] a study for a three-dimensional droplet in channels has been made. The interested readers can refer to [29, 36], for study of the accuracy and range of application of equation (26).

In the present study all the contact angle have been calculated from the Laplace law ($\Delta p = (2\gamma \cos\theta)/H$) and measuring the density contours near the walls. Equation (26) is used only for estimating the contact angle.

4.1. The chemical step case with $\theta_1 = \theta_4$ and $\theta_2 = \theta_3$

In this section we study the dynamics of 2D droplets inside the channels under a chemical step. We will try to compare the numerical results for different conditions, including various heights of the channel, various viscosity ratios and different contact angles, with the analytical results (equations (17) and (18)). We first consider a droplet in position $x = 119$. After 15 000 time steps the equilibrium contact angles becomes equal to θ_1. Then the equilibrium contact angle of the right side changes to θ_2 but there is no change in the interactions of the channel walls on the left side of the channel (G_2 remains unchanged for the left side of the walls). In the following we use $G_{2,\mathrm{r}}$ and $G_{2,\mathrm{l}}$ to refer to the interaction coefficients of the right and the left sides of the chemical step, respectively. Also $t = 0$ in the diagrams refers to the equilibrium situation (15 000 time steps). Considering the physics of the problem, if we use the equilibrium velocity of the droplet u^{e} to define the Reynolds number ($Re = \rho u^{\mathrm{e}} H/\mu$) and capillary number ($Ca = \mu u^{\mathrm{e}}/\gamma$), the range of the Reynolds number will be between 0.1 and 2.0, which indicates that the inertial terms have less effect than viscous terms. In addition, the capillary number changes between 0.01 and 0.02, which is the ratio of viscous terms to the surface tension forces.

4.1.1. The effect of channel height. The channel height is a parameter whose effect on the dynamics can be very important. It should be noted that for 2D droplets, on changing the channel height the total driving force does not change and remains constant. This means that on increasing the height the driving force per unit volume of the droplets decreases [14].

In figure 4 the results for the displacement and center of mass velocity of the droplet are shown for different heights (40 and 60) and have been compared with the analytical predictions, i.e., from equations (17) and (18). In the simulations the density and the viscosity of the fluids were supposed to be equal ($\rho_{\mathrm{l}} = \rho_{\mathrm{g}} = 2$) and ($\mu_{\mathrm{l}} = \mu_{\mathrm{g}} = 1/6$). It should be noted that in both the cases studied, with height 40 and 60, the coefficients related to interactions between the two components with walls remains fixed and only the height changes. Initially for all the channel surfaces $G = 0.2$. After the equilibrium time for regions of the channel with $x > 119$, suddenly the value of $G_{2,\mathrm{r}}$ changes and we have $G_{2,\mathrm{r}} = 0.3$ and $G_{2,\mathrm{l}} = 0.2$. These results show that on increasing the channel height and keeping all the other parameters constant, the dynamics is enhanced and the velocity of the droplet increases. The analytical solution can predict this behavior well and, as depicted in figure 4, the numerical results are in close agreement with the analytical solution. As already reported, the equilibrium contact angle within the channel changes upon increasing the height and the capillary number [33, 37].

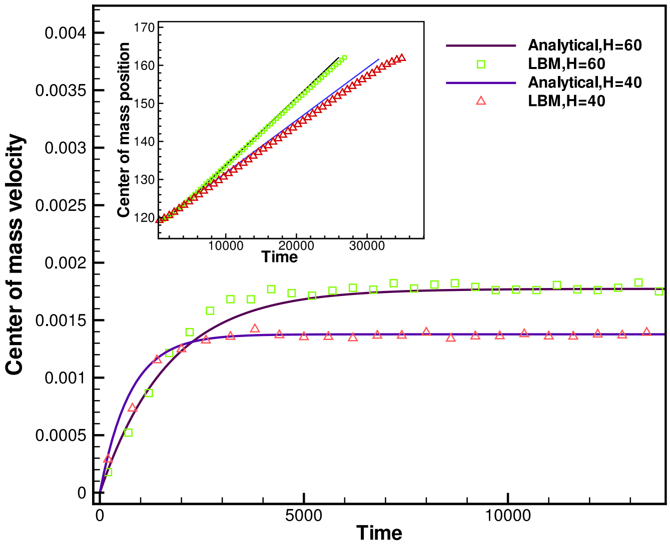

Figure 4. The center of mass velocity of the droplet for two different heights (40, 60) and a comparison of the results with those from the analytical solution. The positions of the center of mass of the droplet versus time are shown in the inset. For $h = 40$ the dynamic contact angles are equal to $\theta_1 = \theta_4 = 59.1^\circ$ and $\theta_2 = \theta_3 = 47.1^\circ$ and for $h = 60$ we have $\theta_1 = 58.3^\circ$ and $\theta_2 = 48.4^\circ$. $G_c = 90$ in all the calculations. Note that the calculated contact angles are the dynamic contact angles.

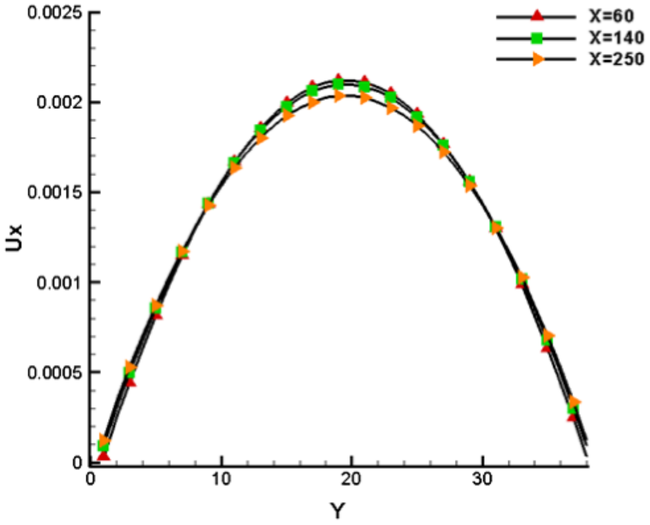

Figure 5. A comparison between the velocity profile obtained from the simulation and the parabolic profile assumed in the analytical section. $H = 40$ and the other parameters are equal to those considered for figure 4.

In figure 5 we have checked the validity of the parabolic profile assumption considered in deriving the analytical relation. As can be seen, for all the three sections ($x = 60$, 140 and 250) the parabolic profile assumption is well borne out. However, our results indicate that on increasing the velocity the deviation grows.

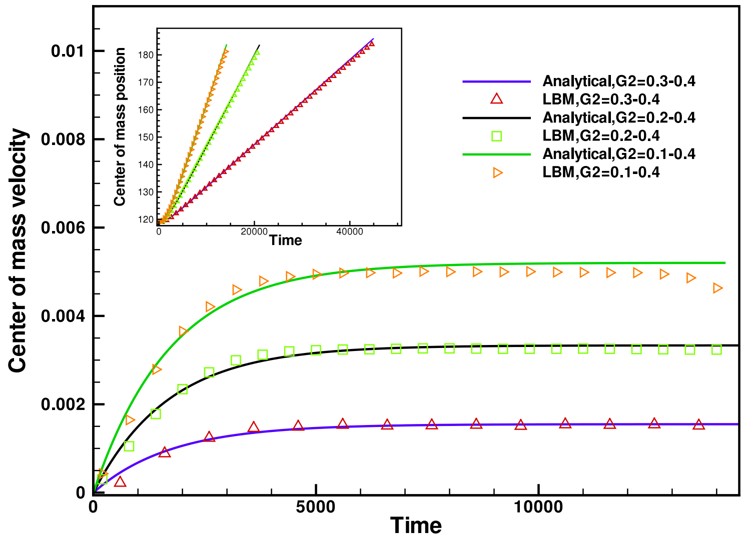

Figure 6. The center of mass velocity of the droplet as a function of time for different wettabilities and a comparison with analytical solutions. The positions of the center of mass are shown in the inset. Throughout the calculation $G_{2,\mathrm{r}} = 0.4$, but $G_{2,\mathrm{l}}$ takes the following values: 0.1, 0.2 and 0.3.

4.1.2. The effect of surface wettability and the contact angle. In this section the effect of wettability and the angle of contact between the parts of the chemical step for various cases are studied. As equations (17) and (18) indicate, the velocity and displacement of the center of mass of the droplet are proportional to the difference of the cosines of the step contact angles. Thus, changes in the contact angles can substantially modify the dynamics. The results shown in figure 6 clearly reveal the effect of the contact angles size on the displacement of the center of mass of the droplet as a function of time. In all the calculations $\rho_\mathrm{l} = \rho_\mathrm{g} = 2$, $\mu_\mathrm{l} = \mu_\mathrm{g} = 1/6$ and $G_{2,\mathrm{r}} = 0.4$, but for these samples the dynamic contact angles are equal to: for the first sample $G_{2,\mathrm{l}} = 0.3$, $\theta_1 = 27.92°$ and $\theta_2 = 40.44°$; for the second sample $G_{2,\mathrm{l}} = 0.2$, $\theta_1 = 33.41°$ and $\theta_2 = 55.3°$; and for the third sample $G_{2,\mathrm{l}} = 0.1$, $\theta_1 = 38.4°$ and $\theta_2 = 68.3°$. As can be concluded from figure 6 the maximum error (3.6%) in predicting the velocity is for the case with $G_{2,\mathrm{l}} = 0.1$. This could be due to the deviation of the behavior of the system from those assumed for deriving the analytical solution at large velocities.

4.1.3. The effect of viscosity. It is well known that at the microscale and nanoscale the Reynolds number is low. This means that viscous forces play an important role in the problem. Therefore, it is necessary to study the effect of the viscosities of both the fluids (fluid 1 and fluid 2) on the dynamics. In this section, similar to section 4.1.2, the results for the dynamics of the droplet are presented for the limiting case of the density and the viscosity (same density and viscosity). Then the viscosity of the first fluid (the main fluid) is considered for double and three times the initial value. It should be noted that one of the problems of the multi-component Shan–Chen method is that the density and viscosity ratio are not independent and on changing the density the viscosity changes [35]. Therefore, it is not possible to accurately adjust the viscosity ratio. Due to this limitation, in the simulation $\tau_2 = 1$ but τ_1 changes, taking the values 1, 1.5 and 2. On this basis,

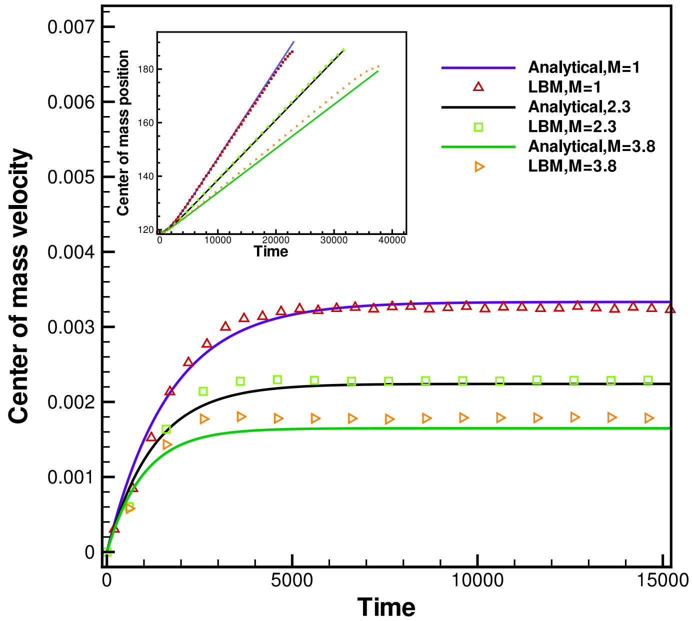

Figure 7. The center of mass velocity of the droplet as a function of time for different viscosities and comparisons with analytical solutions. The positions of the center of mass of the droplet are given in the inset. Throughout the calculation, $G_{\mathrm{c}} = 0.9$ and $\tau_2 = 1$, but τ_1 takes the following values: 1, 1.5 and 2. M also takes the following values: 1, 2.3 and 3.8.

the viscosity ratios for the cases considered are equal to $M = \mu_1/\mu_2 = 1, 2.3$ and 3.8, respectively. In the simulation, $G_{2,\mathrm{l}} = 0.2$ and $G_{2,\mathrm{r}} = 0.4$. Also the relaxation times and densities for the second case are $\tau_1 = 1.5$, $\tau_2 = 1$, $\rho_{\mathrm{g}} = 1.86$ and $\rho_{\mathrm{l}} = 2.13$, and for the third case we have $\tau_1 = 2$, $\tau_2 = 1$, $\rho_{\mathrm{g}} = 2.31$ and $\rho_{\mathrm{g}} = 1.796$. The velocity and center of mass of the droplet for these three cases are depicted in figure 7. As the diagrams show, on increasing the viscosity of the droplet, the velocity and the dynamics of the droplet reduce. In addition, the analytical solution can predict the velocity and the displacement of the droplet well. As is evident, at large viscosities the deviation between the analytical and the numerical results increases (third case). This can be attributed to a finite slip resulting from the bounce-back boundary condition at such viscosities [34]. It is worth noting that an increase in error on increasing the viscosity for some analytical relations has been previously reported [35].

4.2. The chemical step case with $\theta_2 \neq \theta_3 \neq \theta_4$ and $\theta_1 = \theta_4$

The work done for studying the motion of droplets on chemical steps has mostly concentrated on situations where the conditions are equal perpendicular to the channel axis and wettability changes only horizontally along the channel, namely, $\theta_1 = \theta_4$ and $\theta_2 = \theta_3$ [14]. For a thorough study we rather consider a more general case and suppose that the contact angles on the right sides of the top and bottom walls are different, namely, $\theta_2 \neq \theta_3$. To investigate the contact angle effect, all the parameters were kept constant and only the parameter $G_{2,\mathrm{r}}$ for the top wall is changed, and its effect on the center of mass velocity of the droplet is studied. In the calculations, $\rho_{\mathrm{l}} = \rho_{\mathrm{g}} = 2$,

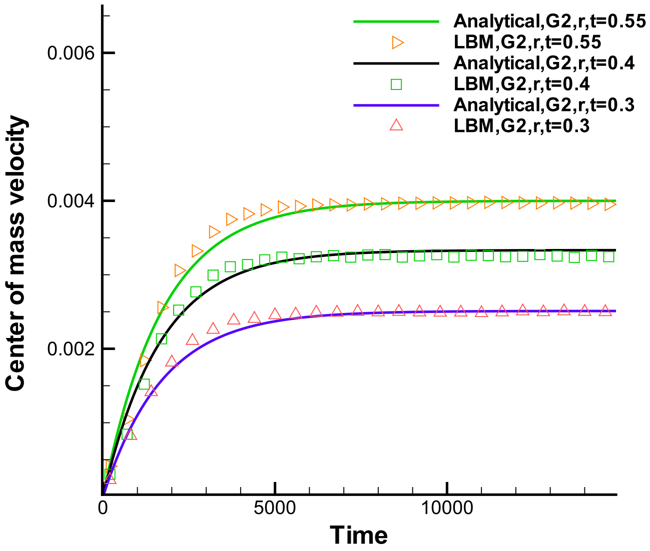

Figure 8. The center of mass velocity of a droplet as a function of time and a comparison with the analytical solutions for an asymmetric condition of the contact angles on the top and bottom walls. $G_{2,\mathrm{l,b}} = G_{2,\mathrm{l,t}} = 0.2$ and $G_{2,\mathrm{r,b}} = 0.4$. $G_{2,\mathrm{l,t}}$ is changed to obtain different values for θ_3.

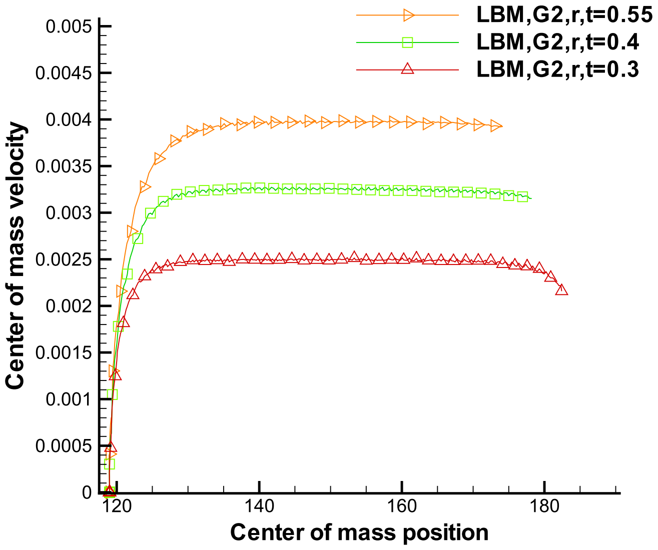

Figure 9. The center of mass velocity of the droplet as a function of its position. $G_{2,\mathrm{l,b}} = G_{2,\mathrm{l,t}} = 0.2$ and $G_{2,\mathrm{r,b}} = 0.4$. $G_{2,\mathrm{r,t}}$ is changed to provide different values for θ_3.

$\mu_\mathrm{l} = \mu_\mathrm{g} = 1/6$, $G_{2,\mathrm{l,b}} = G_{2,\mathrm{l,t}} = 0.2$ and $G_{2,\mathrm{r,b}} = 0.4$, where the subscripts t and b stand for the top and bottom walls, respectively. $G_{2,\mathrm{r,t}}$ takes different values, creating different contact angles (different θ_3). Taking into account the capability of the analytical solution it is straightforward to compare the numerical results with the analytical outcomes. In figure 8 a comparison between the numerical and the analytical results has been performed for the center of mass velocity of the droplet as a function of the time. In figure 9 the

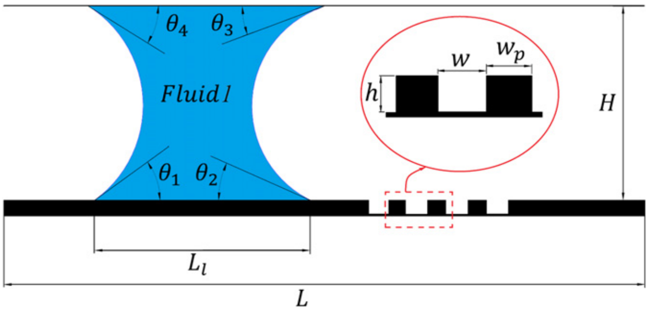

Figure 10. A schematic representation of the situation for the droplet within the channel with grooved surfaces. $\theta_1 = \theta_4$, $\theta_2 = \theta_3$. In all the cases $\tau_2 = 1$ but τ_2 takes the values 0.1, 1.5, 2.0. The grooves have the same height h and width w_p. The distance between the grooves is equal to w.

center of mass velocities versus center of mass positions are shown. As can be concluded from the results of figures 8 and 9 and also from the analytical solution, on increasing the wettability of the right wall, the velocity of the droplet increases.

4.3. The effect of grooves

The effect of grooves on the dynamics of droplets within the channels and also in capillary filling has recently been given attention [16, 17, 22, 23, 38]. In [24, 25], body force driven droplets were considered and the effect of surface grooves and the wetting on the dynamics were investigated via LBM. In this section we consider the effects of the grooves on wettability driven droplets. Figure 10 illustrates the geometrical parameters involved in the problem for studying the effect of grooves. As depicted, for both the top and bottom walls a chemical step is applied and the bottom wall is grooved. We study the effect of height h, distance between the grooves w and width of the grooves w_p on the dynamics. The total numbers of grid points considered in the problem are 300×50 in the horizontal and vertical directions, respectively.

4.3.1. The chemical step on both the channel walls ($\theta_1 = \theta_4$ and $\theta_2 = \theta_3$). We first consider cases where the top and bottom walls are hydrophilic. The contact angles are considered to be $\theta_1 = \theta_4 = 33.37°$ and $\theta_2 = \theta_3 = 55.57°$. Initially the groove widths w_p are kept fixed equal to 8 and the effects of h and w are studied. Then the effect of w_p is investigated. Three grooves with $(h \times w)$ equal to (4×4), (4×8) and 8×4 are the three samples that we have considered.

Figure 11 shows that on increasing the distance between the grooves from four to eight lattice units, the maximum velocity approximately remains the same but the minimum velocity is reduced more when the distance is larger. This can be associated with the larger distance that the droplet should move to fill the grooves. Also on increasing the height, the velocity of the droplet decreases. This indicates an increase of the drag with height because the fluid should occupy larger space and, as a result, its velocity decreases. Similar behavior has also been observed for droplets under a volumetric force [25]. It should be noted that the first peak in figure 11 is the result of a chemical step on the smooth surface which is shown in figure 10. Now the effect of w_p will be studied. In figure 12 the velocity

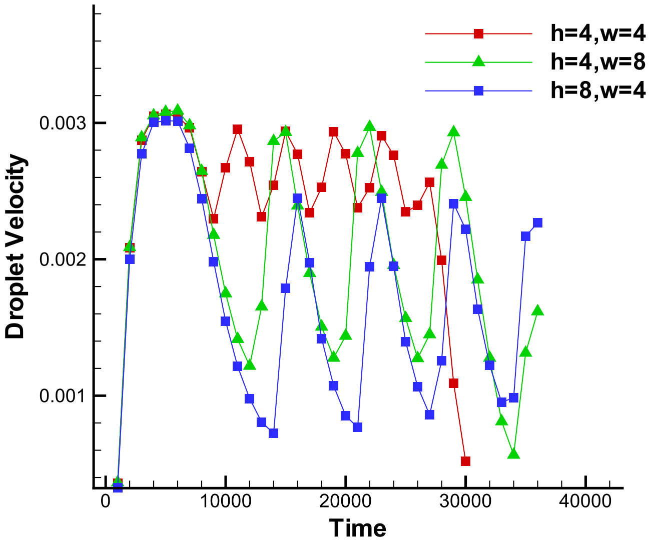

Figure 11. Velocity changes of the center of mass of the droplet on grooved and hydrophilic surfaces and the effect of the height and the distance between the grooves on the dynamics. $\rho_\mathrm{l} = \rho_\mathrm{g} = 2$ and $\mu_\mathrm{l} = \mu_\mathrm{g} = 1/6$ and $G_\mathrm{c} = 0.9$.

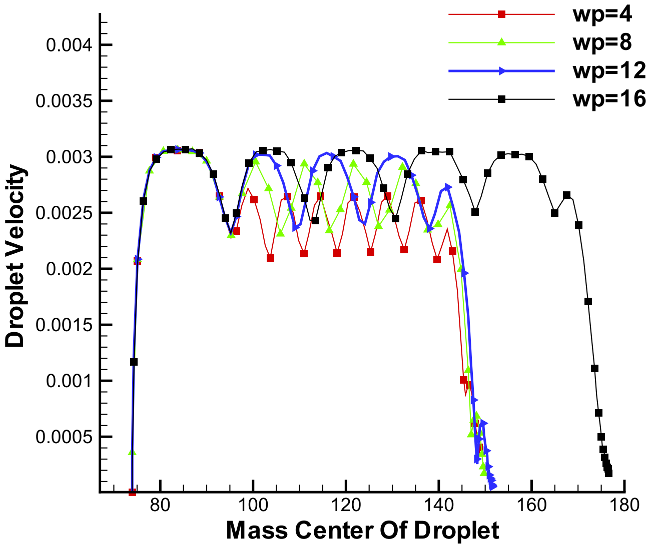

Figure 12. Velocity changes of the center of mass of the droplet on hydrophilic surfaces and the effect of the width of the grooves on the dynamics. $\rho_\mathrm{l} = \rho_\mathrm{g} = 2$ and $\mu_\mathrm{l} = \mu_\mathrm{g} = 1/6$ and $G_\mathrm{c} = 0.9$.

of the droplet as a function of the position of the center of mass of the droplet is given for different values of w_p. The height and the distance between the grooves are equal to 4. From the results of figure 12 it can be seen that on increasing the distance of the grooves the velocity of the droplets increases and tends to the equilibrium velocity over a smooth surface. This is an expected result, as on increasing the distance the droplets have more time to reach their previous dynamic contact angle. However, for grooves with

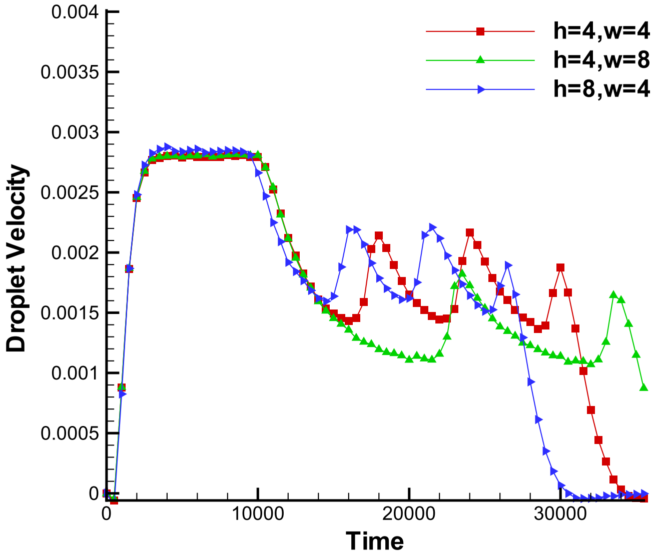

Figure 13. Velocity changes of the center of mass of the droplet on hydrophobic surfaces and the effect of the height and the distance between the grooves on the dynamics. $\rho_{\mathrm{l}} = \rho_{\mathrm{g}} = 2$ and $\mu_{\mathrm{l}} = \mu_{\mathrm{g}} = 1/6$ and $G_{\mathrm{c}} = 0.9$.

less distance the droplets are not able to retrieve their profile and quickly enter the next groove, and this reduces the velocity.

Now we assume that the top and bottom walls are hydrophobic. The contact angles are $\theta_1 = \theta_4 = 123.8°$ and $\theta_2 = \theta_3 = 145.59°$. Like in the previous part we will consider the effect of the distance between the grooves. Figure 13 shows that on increasing the distance from four to eight lattice units the maximum velocity smoothly reduces. This behavior contrasts with the behavior observed for hydrophilic surfaces. Also increasing the height does not change the maximum velocity appreciably. In hydrophilic surfaces the front edge of the droplet can touch the bottom of the grooves but in hydrophobic surfaces the front edge jumps from one groove to another groove and does not touch the bottom of the groove.

Now we consider the effect of groove width on the dynamics. Four different widths (4, 8, 12 and 16) are considered in the study and the height and distance between the grooves are supposed to be constant, equal to 4. The results are presented versus center of mass of the droplet in figure 14. It can be seen that for a hydrophobic surface, on increasing the width, the velocity of the droplet reaches its initial value.

A relation that can be used to estimate the contact angle on chemical substrates is the Cassie relation that is given as [39]

$$\cos\theta_{\mathrm{c}} = (1 - r)\cos\theta_0 - r, \tag{27}$$

where θ_{c} is the contact angle on chemical substrates, θ_0 represents the contact angle on homogeneous substrates and $r = w/(w + w_p)$. It is seen that on increasing w_p, r reduces and the contact angle tends to that of a smooth surface. This can explain the velocity increasing and reaching that of a smooth surface when w_p increases.

In summary, it can be concluded that for hydrophilic surfaces, changing the distance between the grooves does not change the dynamics appreciably and the velocity of the

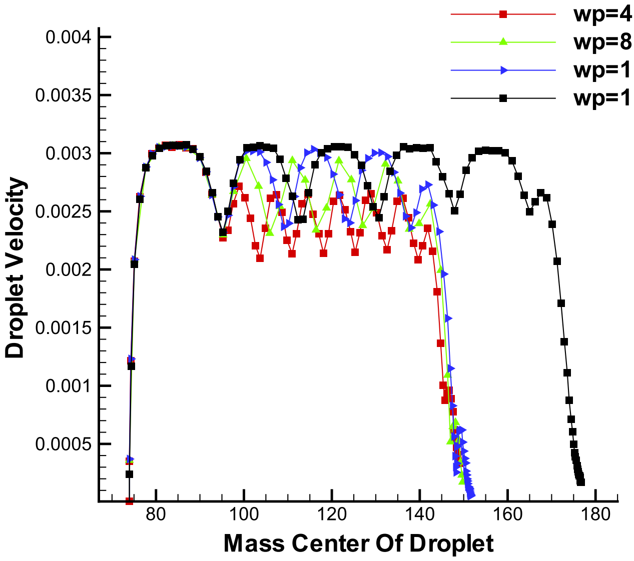

Figure 14. Velocity changes of the center of mass of the droplet on hydrophobic surfaces and the effect of the width of the grooves on the dynamics. $\rho_l = \rho_g = 2$, $\mu_l = \mu_g = 1/6$ and $G_c = 0.9$.

droplet after each groove reaches its initial value. However, for hydrophobic surfaces, on increasing the distance the velocity decreases. Increasing the height of the grooves weakens the dynamics for hydrophilic surfaces but for hydrophobic surfaces the dynamics does not change appreciably.

4.3.2. The chemical step on the top wall ($\theta_1 = \theta_2$). In all the simulations done so far, chemical step heterogeneity is applied for both the top and the bottom walls. Here we suppose that the chemical step is applied on the top wall only. The interaction coefficients for the right and the left parts of the top wall are $G_{2,r,t} = 0.55$ ($\theta_3 \approx 10°$) and $G_{2,l,t} = -0.1$ ($\theta_4 \approx 102°$). Three situations for the bottom wall were considered, namely, $\theta_1 = \theta_2 = 59.2°$, $\theta_1 = \theta_2 = 90°$ and $\theta_1 = \theta_2 = 111.3°$. As illustrated in figure 15, in all the cases the droplet is pinned on the bottom wall and does not move further, while on the top wall, the droplet is stretched. This behavior continuous throughout the simulation until the droplet on the top wall reaches the end of the side of the simulation domain.

4.4. The effect of obstacles on the dynamics ($\theta_1 = \theta_4, \theta_2 = \theta_3$)

Obstacles are considered in the channels for different purposes including breakup of a droplet into two smaller droplet. In this section we investigate the effect of an obstacle on the dynamics. As depicted in figure 16, a rectangular obstacle with width h_0 and length L_0 is placed in the middle of the channel. In the simulation all the contact angles of the obstacle were supposed to be 90°. The parameters involved in the problem are $\rho_l = \rho_g = 2$, $\mu_l = \mu_g = 1/6$, $G_{2,l} = 0.1$ and $G_{2,r} = 0.4$. It is more appropriate to define a non-dimensional parameter $\bar{h} = h_0/H$ and present the results on the basis of this parameter. Figure 17 depicts the displacement of the center of mass of the droplet as a function of time. For both the top and bottom walls the chemical step is considered. L_0 was supposed to be

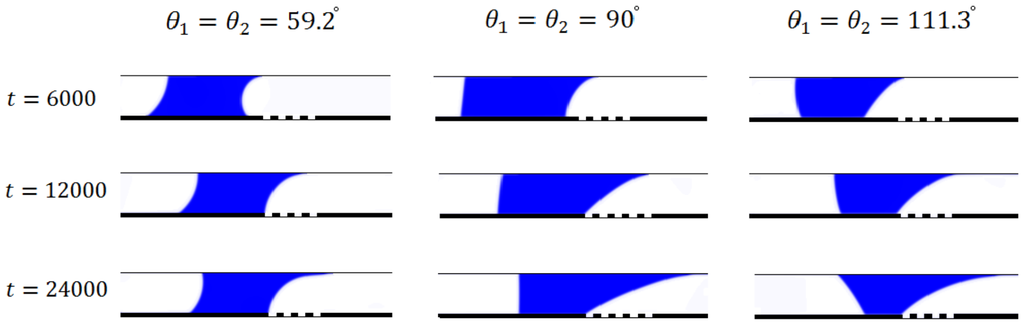

Figure 15. The droplet situation within the channel for three different cases and for different times ($t = 6000, 12\,000$ and $24\,000$). θ_1 and θ_2 ($\theta_1 = \theta_2$) take values of 59.2°, 90° and 111.3° for the three cases. The step gradient is only applied on the top surface.

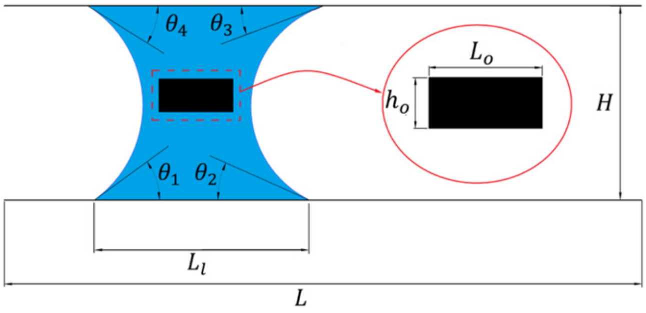

Figure 16. A schematic representation of the droplet within a channel with an obstacle. $\theta_1 = \theta_4$ and $\theta_2 = \theta_3$. The rectangular obstacle has length equal to L_0 and height equal to h_0. The height of the channel is equal to H.

constant, equal to 40, but $\bar{h}$ was changed from 0.2 to 0.7. As depicted in figure 17, on increasing $\bar{h}$ the dynamics weakens. An examination of figure 17 reveals that in almost all of the cases, after a certain time the slope of the curves becomes slower. This change of the slope occurs when the droplet breaks up into two parts and this increases the total solid–fluid surface, and as a result the drag force exerted on the droplet. Figure 18 displays the situation for the droplet before, during and after breakup of the droplets. A comparison between the results of figures 17 and 18 confirms this fact that the change in the slope occurs exactly when the droplet breaks up into the parts.

5. Conclusion

We studied the dynamics of droplets inside microchannels under surface forces created by the chemical steps on the channel walls. A multi-component Shan–Chen lattice Boltzmann method was used for this purpose. The effects of parameters such as the channel height, viscosity and density ratio on the results were investigated for smooth and grooved substrates. Also, an analytical solution was developed for droplets under chemical heterogeneities in the channels with smooth surfaces. The solution considers a

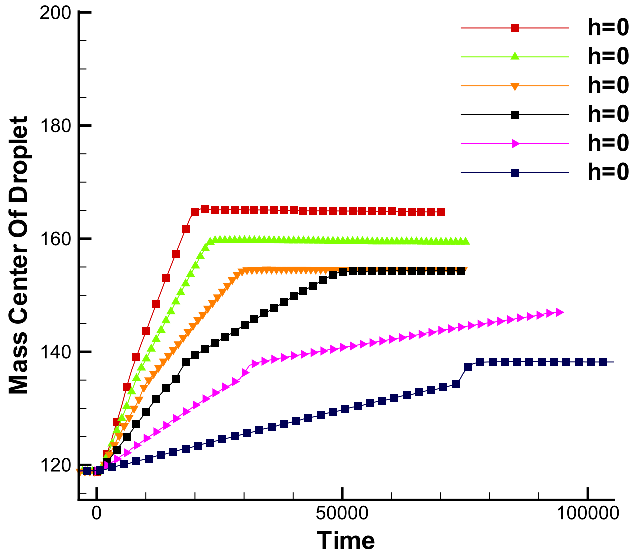

Figure 17. Changes of the center of mass of the droplet for different values of $\bar{h}$ as a function of time. $\rho_{\rm l} = \rho_{\rm g} = 2$, $\mu_{\rm l} = \mu_{\rm g} = 1/6$. The coefficients for the top and bottom walls are equal to $G_{2,{\rm r}} = 0.4$ and $G_{2,{\rm l}} = 0.1$.

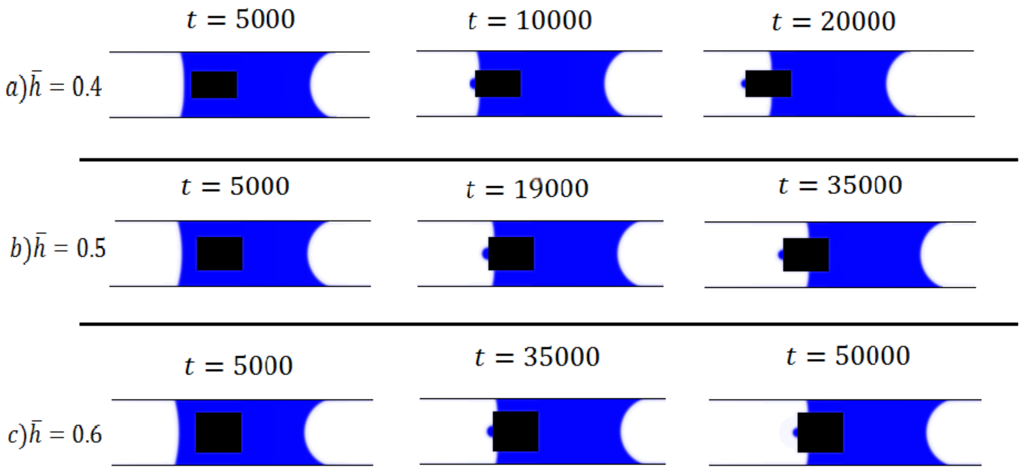

Figure 18. The situation for the droplet inside the channel with the obstacle before, during and after the change of the displacement slope (see figure 17) for different heights of the obstacle. In cases a, b and c, $\bar{h}$ is equal to 0.4, 0.5 and 0.6, respectively.

general condition, namely, asymmetry of the contact angles on the top and bottom walls, the viscosity of the gas as the second fluid and the effect of the channel height.

As can be concluded from equations (17) and (18), on increasing the height the dynamics is enhanced. It should be noted that on increasing the height, the driving force per unit volume of the droplets decreases [14], but on increasing the height, the total driving force does not change and the dynamics is affected by other parameters such as the velocity gradient near the walls (which is a function of the channel height: $\partial u/\partial y|_{y=0} = 6\bar{u}/H$). Then using the Shan–Chen lattice Boltzmann method, the effects of height, viscosity ratio and wettability pattern on different cases were studied and were compared with the analytical solution. Close agreement between the results was observed.

Due to the importance of grooved surfaces we then considered channels with grooves with different sizes on hydrophilic and hydrophobic surfaces. It was found that on increasing the height of the grooves, the drag increases, similar to the case with a constant volumetric force. However, increasing the distance between the grooves (w) does not affect the maximum velocity. The dynamics of droplets on hydrophobic surface was also investigated. In contrast to the case for hydrophilic surfaces, on increasing the distance between the grooves the dynamics weakens. The effect of the width of the grooves on the dynamics was studied for both the hydrophilic and hydrophobic surfaces. If the heterogeneity is applied only on the top surface, the droplets are pinned on the grooves and cannot move further regardless of whether the bottom wall is hydrophilic or hydrophobic.

Finally we studied the dynamics of the droplets in the channels in the presence of an obstacle. The effect of the geometry on the displacement of the droplet was investigated and discussed. The results indicate that on applying a chemical step and making local changes in the contact angles, the droplets can be transported even in the presence of an obstacle.

J. Stat. Mech. (2012) P10005

References

[1] Berthier J, 2008 *Microdrops and Digital Microfluidics* (Norwich, NY: William Andrew)
[2] Chakrabarty K and Su F, 2007 *Digital Microfluidic Biochips: Synthesis, Testing, and Reconfiguration Techniques* (London: Taylor and Francis)
[3] Halverson J D, Maldarelli C, Couzis A and Koplik J, 2008 *J. Chem. Phys.* **129** 164708
[4] Darhuber A and Troian S M, 2005 *Annu. Rev. Fluid Mech.* **37** 425
[5] Raphael E, 1988 *C. R. Acad. Sci.* **306** 751
[6] Chaudhury M K and Whitesides G M, 1992 *Science* **256** 1539
[7] Brochard F, 1989 *Langmuir* **5** 432
[8] Greenspan H P, 1978 *J. Fluid Mech.* **84** 125
[9] Moosavi A and Mohammadi A, 2011 *J. Phys.: Condens. Matter* **23** 085004
[10] Daniel S, Chaudhury M K and Chen J C, 2001 *Science* **291** 633–6
[11] Lee J H, Kim H G, Khang G S, Lee H B and John M S, 1992 *J. Colloid Interface Sci.* **151** 563570
[12] Yamada R and Tada H, 2005 *Langmuir* **21** 4254
[13] Lee S W and Laibinis P E, 2000 *J. Am. Chem. Soc.* **122** 5395
[14] Varnik F *et al,* 2008 *Phys. Fluids* **20** 072104
[15] Varnik F *et al,* 2011 *J. Phys.: Condens. Matter* **23** 184112
[16] Dupuis A and Yeomans J M, 2005 *Langmuir* **21** 2624
[17] Dupuis A and Yeomans J M, 2006 *Europhys. Lett.* **75** 105
[18] Huang J J, Shu C and Chew Y T, 2008 *J. Colloid Interface Sci.* **328** 124
[19] Gong S and Cheng P, 2012 *Comput. Fluids* **53** 93
[20] Hwang H J and Simon Song S, 2008 *Biochip J.* **2** 123
[21] Yang J T, Fang W F and Tung K Y, 2008 *Chem. Eng. Sci.* **63** 1871
[22] Verberg R, Pooley C M, Yeomans J M and Balazs A C, 2004 *Phys. Rev. Lett.* **93** 184501
[23] Zhang R L and Kwok D Y, 2006 *Langmuir* **22** 4998
[24] Zhang R L, Di Q F, Wang X-L and Gu C-Y, 2010 *J. Hydrodynamics* **22** 366
[25] Huang J J, Shu C and Chew Y T, 2009 *Phys. Fluids* **21** 022103
[26] Shan X and Chen H, 1993 *Phys. Rev.* E **47** 1815
[27] Shan X and Chen H, 1994 *Phys. Rev.* E **49** 2941
[28] Martys N S and Chen H D, 1996 *Phys. Rev.* E **53** 743
[29] Huang H, Thorne D T, Schaap M G and Sukop M C, 2007 *Phys. Rev.* E **76** 066701
[30] Benzi R, Sbragaglia M, Succi S, Bernaschi M and Chibbaro S, 2009 *J. Chem. Phys.* **131** 104903
[31] Shan X and Doolen G, 1995 *J. Stat. Phys.* **81** 379
[32] Shan X and Doolen G D, 1996 *Phys. Rev.* E **54** 3614

[33] Chibbaro S, Biferale L, Diotallevi F and Succi S, 2009 *Eur. Phys. J. Spec. Top* **171** 223
[34] Varnik F, Dorner D and Raabe D, 2007 *J. Fluid Mech.* **573** 191
[35] Huang H, Wang L and Lu X-Y, 2011 *Comput. Math. Appl.* **61** 3606
[36] Schmieschek S and Harting J, 2011 *Commun. Comput. Phys.* **9** 1165
[37] Dos Santos L, Wolf F and Philippi P, 2005 *J. Stat. Phys.* **121** 197
[38] Chibbaro S, Biferale L, Binder K, Dimitrov D, Diotallevi F, Milchev A and Succi S, 2009 *J. Stat. Mech.* P06007
[39] De Gennes P G, Brochard-Wyart F and Quéré D, 2003 *Capillarity and Wetting Phenomena: Drops, Bubbles, Pearls, Waves* (Heidelberg: Springer)